

#### Contents lists available at ScienceDirect

# Geoderma

journal homepage: www.elsevier.com/locate/geoderma





# Potassium isotopic fractionation in a humid and an arid soil–plant system in Hawai'i

Wenshuai Li $^a$ , Xiao-Ming Liu $^{a,*}$ , Yan Hu $^b$ , Fang-Zhen Teng $^b$ , Yong-Feng Hu $^c$ , Oliver A. Chadwick $^d$ 

- <sup>a</sup> Department of Geological Sciences, University of North Carolina-Chapel Hill, NC 27599-3315, United States
- b Isotope Laboratory, Department of Earth and Space Sciences, University of Washington, Seattle, WA 98195-1310, United States
- Canadian Light Source, University of Saskatchewan, Saskatoon S7N 2V3, Canada
- <sup>d</sup> Department of Geography, University of California, Santa Barbara, CA 93106, United States

#### ARTICLEINFO

Handling Editor: Jan Willem Van Groenigen

Keywords:
Biogeochemistry
Climate
Source
Aerosol
Phase
Synchrotron Radiation

#### ABSTRACT

Plants play a critical role in the cycling of potassium (K) and the fractionation of its isotopes. However, little is known about K stable isotopic compositions in natural soil-plant systems and possible fractionation during intraplant transport and root-soil uptake of K. This study focuses on K isotopic fractionation within a humid and an arid soil-plant system sampled on the windward and leeward sides of Kohala Mountain, Hawai'i. We determined the K isotopic compositions of < 2-mm bulk soil, soil saturation extraction, and selected plant tissues by multicollector inductively coupled plasma mass spectrometry and X-ray absorption spectroscopy. We studied soils and individual tissue samples such as roots, stems, barks, shoots (a sum of stems and fresh leaves), leaves (fresh and dead), seeds, and flowers of trees and grasses. The results demonstrated that: (i) tissue  $\delta^{41}$ K values ranged from  $-1.06 \pm 0.06$  to  $1.15 \pm 0.09\%$ ; (ii) within the same plant, stems (barks), dead leaves, and reproductive tissues (flowers and seeds) were isotopically lighter compared to fresh leaves, and to a lesser extent, roots; (iii)  $\delta^{41}$ K values of the humid soil (-0.54  $\pm$  0.07 to -0.49  $\pm$  0.06%) were lower than those of the arid soil (-0.24  $\pm$  0.07 to  $-0.14\pm0.06$ %); and (iv) soil bioavailable pool  $\delta^{41}$ K (saturation extracts) ranged from  $-0.63\pm0.08$  to  $0.34\pm0.06$ 0.08‰ and 0.48  $\pm$  0.08 to 0.54  $\pm$  0.10‰ in the humid and arid soils, respectively. From synchrotron-based analysis of K atoms, we identified two major K-bearing phases co-existing as ionic K<sup>+</sup> and K-pectate association of different fractions. Based on K isotopic and synchrotron data, we conclude that two dominant processes are responsible for plant-mediated K isotopic fractionation, including (1) K redistribution during intra-plant circulation and (2) uptake at the root-soil interface. For intra-plant circulation of K, there is a high affinity of isotopically lighter K to organic complexes as K-pectate, and K-pectate is particularly enriched in roots and fresh leaves. For K uptake at root-soil interface, isotopically lighter K is preferentially taken by roots from soil bioavailable pools following a low-affinity (passive) transport path. Soil K budget in two sites reflects strong source mixing effects with limited plant imprints. This work provides exploratory data on the biogeochemical fractionation of K isotopes in the soil-plant system.

#### 1. Introduction

Vegetation influences the K biogeochemical cycle by enhancing its weathering release, biological uptake, and bio-cycling (Alexandre et al., 1997; Song et al., 2012). Potassium plays an important role in metabolic and physiological processes during plant growth and development, such as photosynthesis, enzyme activation and osmoregulation (Shabala, 2003; White and Karley, 2010). Plant roots can take up K from soil

solution via mass flow during transpiration. Soil solution (bioavailable pool) K is supplied via (i) leaching from the canopy and stem by rainwater; (ii) release from decaying organic materials; (iii) mineral weathering; (iv) dry deposition of K-containing aerosols on plant outer surfaces and lateral wash-off; and (v) wet deposition of K-bearing rainwater particularly for studied Hawaiian Islands (Chadwick et al., 1999; Holmqvist et al., 2003; Weis and Weis, 2004; Kayser and Isselstein, 2005; Tripler et al., 2006; Chaudhuri et al., 2007; Kopáček et al., 2009).

E-mail address: xiaomliu@unc.edu (X.-M. Liu).

<sup>\*</sup> Corresponding author.

For acidic, highly-weathered soils, long-term weathering of K-bearing minerals and leaching probably limits the availability of K, particularly on K-poor parent substrates (e.g., Tripler et al., 2006; Sardans and Peñuelas, 2015). Loss of soil K contributes up to ~ 70% of dissolved K in global rivers (Chaudhuri et al., 2007).

Plants fractionate stable isotopes in macronutrients as Ca and Mg and micronutrients like Cu, Fe, and Zn (e.g., Weiss et al., 2005; Guelke and Von Blanckenburg, 2007; Bolou-Bi et al., 2010; Caldelas et al., 2011; Cobert et al., 2011; Jouvin et al., 2012; Schmitt et al., 2013; Christensen et al., 2018). The stable K isotope ratio ( $^{41}\text{K/}^{39}\text{K}$ ) has been measured in extraterrestrial silicates (Humayun and Clayton, 1995), terrestrial rocks and lunar soils (Humayun and Koeberl, 2004), barley plants (Becker et al., 2008), and animals including bioproducts (Murphy et al., 2002). However, distinguishing K isotopic fractionation in natural soil-plant systems has relied on laborious isotope spiking treatment to reach the required analytical precision. Recent advances in analytical methods using multi-collector inductively coupled plasma mass spectrometry (MC-ICP-MS) allows for high-precision measurement (optimal 2S.D. better than 0.06%) of stable K isotope ratios (expressed in a  $\delta$  notation, per-mille) to determine K isotopic fractionation produced by Earth's surface processes (e.g., Li et al., 2016; Morgan et al., 2018; Hu et al., 2018; Chen et al., 2019; X. Li et al., 2020c; Moynier et al., 2021).

Stable K isotopes are fractionated during chemical weathering and biological cycling (e.g., Santiago Ramos et al., 2018; S. Li et al., 2019a, 2021a, 2021b; Chen et al., 2020; Huang et al., 2020; Teng et al., 2020). Considerable K isotopic fractionation between plants and igneous rocks (taken as the K sources) ( $\Delta^{41}$ K<sub>Plant-Rock</sub>) of  $\sim 0.8$ % was reported in Li et al. (2017), suggesting that terrestrial plants mostly prefer isotopically light K; however this interpretation is equivocal because the source of plant K was not reported. Recently, Morgan et al. (2018) documented isotopically heavier K in commercial banana fruits ( $\Delta^{41}$ K<sub>Plant-Seawater</sub>  $\sim$ 0.4‰) and lighter K in potato tuber ( $\Delta^{41}K_{Plant\text{-}Seawater} \sim 0.1$ ‰), in comparison with the modern seawater (homogeneous  $\delta^{41}K \sim 0.14\%$ , Hille et al., 2019; Wang et al., 2020). Such a comparison with seawater is used in this instance because K fertilizers are often produced by marine evaporates (Barker and Pilbeam, 2016; Li, 2017). By contrast, Christensen et al. (2018) reported partitioning of light K isotopes ( $\Delta^{41}$ K<sub>Source</sub>-Plant up to 1.67%) into different types of crops (soybean, rice, and wheat) from cultured media in hydroponic experiments. So far, few plant species have been investigated, and we know little about the mechanisms of K isotopic fractionation in terrestrial ecosystems.

In this study, we investigate K speciation and K isotopic composition in trees (*Macadamia integrifolia* Maiden & Betche; *Prosopis chilensis* (Mol.) Stuntz) and grasses (*Pennisetum setaceum* (Forssk.) Chiov.; *Cenchrus ciliaris* L.) sampled from a humid and an arid soil–plant system in Hawai'i. We determine the variations in soil-root and intra-plant K isotopic fractionation and evaluate the controlling mechanism. Our aim is to understand K isotopic fractionation in two natural soil–plant systems by measuring the isotopic composition of soils and plant tissues. Furthermore we evaluate the location of K within plant tissues by using synchrotron measurements to model the immediate chemical environment associated with plant K.

## 2. Geology and materials

Kohala Mountain is the northwestern-most and the oldest volcano making up the Island of Hawaiʻi (McDougall, 1964). It has a strong windward-leeward contrast in rainfall, which is useful for evaluating climatic influences on chemical weathering (Chadwick et al., 2003). Two chemically distinct lavas are exposed on Kohala Mountain: 1) the Pololū lava that is composed mainly of tholeiitic basalts  $\sim 350~{\rm ka}$  in age, and 2) the Hāwī lava that forms an alkalic cap over the central region of the mountain  $\sim 150~{\rm ka}$  in age (Spengler and Garcia, 1988; Chadwick et al., 2003). The ages of the regoliths are difficult to constrain, and we considered the radiometric age of the lava flows to be equivalent to the duration of silicate weathering because the constructional surface of

lava flows was minimally eroded.

We sampled two sites receiving different mean annual precipitation (MAP) on the Pololū substrate, which were originally sampled by Goodfellow et al. (2014) (Fig. S1). Each site supports plant species introduced for commercial purposes (Fig. S2). Specifically, the humid site (BE, forest) is located at the intersection of Highway 270 and Iole road (Iole Ahupua'a) (Location: N20.2288, W-155.7896; MAP of 1730  $\pm$  57 mm·a $^{-1}$ ), densely covered with pasture grasses and macadamia trees. The arid site (PO, grassland) is located on Highway 270 between Mahukona and Kaiwaihae in the Kaiholena Ahupua'a (Location: N20.1357, W-155.8859; MAP of 385  $\pm$ 53 mm·a $^{-1}$ ) and supports buffelgrass and mesquite.

Mean annual rainfall data are derived from the University of Hawai'i's digital climate map (Giambelluca et al., 2013). In response to local climate, the soil properties of the two sites differ in terms of weathering depth and leaching intensity but are similar in mineralogy assemblage except that the arid site exhibits development of a calcareous layer (calcite and dolomite) at ~ 1-m depth (Capo et al., 2000; Goodfellow et al., 2014). We collected the following plant species: M. integrifolia (Macadamia nut tree) and P. setaceum (Fountain grass) in the humid site, and P. chilensis (Chilean mesquite tree) and C. ciliaris (Buffel-grass) in the arid site. Although we have no direct knowledge of fertilizer additions to the sampling sites, local experts told us that K fertilization was not been common on lands similar to the sparsely vegetated dry site or on the macademia nut orchard on the wet site. In addition, we found no direct evidence of anomalous K addition (e.g., elevated K concentrations) in soils based on published elemental and Sr isotopic data in soil NH<sub>4</sub>Ac extracts (exchangeable pools) in Hawai'i (Whipkey et al., 2000; Chadwick et al. 2009; Li et al., 2020a). Therefore, anthropogenic impacts should be minor. Based on soil features as color, mineralogy, and gains (losses) of elements (Li et al., 2020a), we separated the soil into two soil depth layers (the topsoil, 0-30 cm; the subsoil, 30-100 cm)—the shallower layer corresponds to stronger biological influences and the deeper one is more strongly influenced by the basalt substrate (see Ziegler et al., 2005; Vitousek and Chadwick, 2013). In sum, three sets of samples were collected from the field, and details are given below.

The first suite of samples—designed to investigate potential K sources—includes parent basalt substrate (Pololū basalts) and the more recent Hāwī tephra that may have been incorporated into the older Pololū soils (i.e., collectively called "basaltic substrate"). Since previous studies demonstrate contribution of Asian dust to Hawaiian soil cation budgets (e.g., Chadwick et al., 1999; Kurtz et al., 2001; Li et al., 2020a; Vogel et al., 2021), we consider K from that source as well. A likely source for Asian dust is the Chinese Loess Plateau (CLP) (An et al., 1990), so we tentatively use data from a Chinese loess sample JX-1 (Huang et al., 2020) to characterize possible K contribution from this source. We use the term "mineral aerosol" instead of "dust" for this long-distance transported material.

The second suite of samples was designed to investigate the interaction among soil-plant systems. It includes rainwater (filtered) collected during separate rainfall events, bulk soils (<2mm size, the topsoil and subsoil), and soil saturation extracts (see Methodology for details) (Table 1). Biologically available K in soil can be extracted using this method. Soil waters were not collected because it is hard to use lysimeters for soil water collection in the arid site, and the installation probably disturbs soil integrity and causes preferential flow pathway resulting in perturbed, unrepresentative infiltration of porewater (Uhlig et al., 2020). Rainfall samples were collected with a plastic funnel inserted into a 2-L Erlenmeyer flask (acid-washed using 1 M HCl followed by rinses with deionized water). The humid soil was classified as very-fine, parasesquic, isohyperthermic Typic Humustepts, and the arid soil was classified as fine, mixed, semiactive, isohyperthermic Sodic Haplocambids (Soil Survey Staff, 2014). The physicochemical properties of the two soils were reported in Li et al. (2020a). Coarse particulate organic matter and root residues were manually removed during soil

**Table 1**A summary of sampling information including locations, types, species and potassium chemistry.

Туре	Sample locations, types, and species	No.	Height above surface (cm)	$K(g \cdot kg^{-1})$	$\delta^{41}$ K (‰)	2S.D. (‰)	N	$\Delta^{41}$ K <sub>Plant-Source</sub> (‰)
Water	Filtered rainwater (2018 October)	W-1	n.d.	n.d.	-0.21	0.11	7	n.d.
	Filtered rainwater (2019 July)	W-2	n.d.	n.d.	-0.16	0.07	7	n.d.
	Hāwī tephra	W-3	n.d.	8.4	-0.48	0.10	6	n.d.
	Pololū basalt	W-4	n.d.	8.1	-0.48	0.04	7	n.d.
Trees	Humid M. integrifolia fresh leaf (2019 July)	B-1	150	4.9	1.07	0.10	5	1.22
	Replicate	B-1	150	n.d.	1.15	0.09	5	1.30
	Averaged value	B-1	150	4.0	1.11	0.10	5	1.26
	Humid M. integrifolia dead leaf (2019 July)	B-2	150	1.6	0.34	0.07	5	0.49
	Humid M. integrifolia bark (2019 July)	B-3	140	3.3	-1.06	0.06	7	-0.92
Grasses	Humid P. setaceum seed (2018 October)	B-4	30	20.1	-0.74	0.07	5	-0.60
	Humid P. setaceum flower (2018 October)	B-5	30	18.3	-0.62	0.05	7	-0.48
	Humid P. setaceum fresh leaf (2019 July)	B-6	10-30	26.8	-0.43	0.06	5	-0.29
	Humid P. setaceum fresh shoot (2019 July)	B-7	0–30	25.8	-0.46	0.04	6	-0.32
	Humid P. setaceum fresh root (2018 October)	B-8	(-40) - 0	9.0	-0.5	0.07	7	-0.36
	Humid P. setaceum fresh shoot (2018 October)	B-9	0–30	24.3	-0.39	0.07	7	-0.25
	Humid P. setaceum dead leaf (2019 July)	B-10	10-30	2.0	-1.03	0.08	7	-0.89
	Humid P. setaceum stem (2019 July)	B-11	0–10	21.4	-0.6	0.07	5	-0.46
	Humid P. setaceum root (2019 July)	B-12	(-40) - 0	10.0	-0.54	0.07	7	-0.40
	Humid P. setaceum root HCl extracts (2019 July)	B-13	(-40) - 0	n.d.	0.29	0.07	7	n.d.
Soil and extracts	Humid topsoil	B-14	(-30) - 0	28.7	-0.49	0.06	7	n.d.
	Soil saturation extracts	B-15	(-30) - 0	n.d.	0.34	0.08	6	n.d.
	Humid subsoil	B-16	(-100) - (-30)	8.7	-0.54	0.07	6	n.d.
	Soil saturation extracts	B-17	(-100) - (-30)	n.d.	-0.63	0.08	6	n.d.
Trees	Arid P. chilensis fresh leaf (2019 July)	P1	150	8.9	0.22	0.05	5	-0.29
	Replicate	P1	150	n.d.	0.20	0.05	5	-0.31
	Averaged value	P1	150	8.9	0.21	0.05	5	-0.30
	Arid P. chilensis dead leaf (2019 July)	P2	150	2.1	-0.63	0.06	7	-1.14
	Arid P. chilensis bark (2019 July)	Р3	140	2.9	-0.01	0.06	7	-0.52
	Replicate	Р3	140	n.d.	0.07	0.05	7	-0.44
	Averaged	Р3	140	n.d.	0.03	0.05	7	-0.48
Grasses	Arid C. ciliaris fresh leaf (2019 July)	P4	10-30	11.5	0.41	0.05	5	-0.10
	Replicate	P4	10-30	n.d.	0.53	0.04	5	0.02
	Averaged value	P4	10-30	11.5	0.47	0.05	5	-0.04
	Arid C. ciliaris fresh shoot (2019 July)	P5	0-30	10.7	0.35	0.05	6	-0.16
	Arid C. ciliaris fresh root (2018 October)	P6	(-30) - 0	4.2	0.25	0.06	7	-0.26
	Arid C. ciliaris fresh shoot (2018 October)	P7	0–30	9.5	0.34	0.07	6	-0.17
	Arid C. ciliaris dead leaf (2019 July)	P8	10-30	1.5	-0.35	0.08	8	-0.86
	Arid C. ciliaris stem (2019 July)	P9	0–10	7.7	0.13	0.08	5	-0.38
	Arid C. ciliaris roots (2019 July)	P10	(-30) - 0	4.0	0.22	0.06	7	-0.29
	Arid C. ciliaris root HCl extracts (2019 July)	P11	(-30) - 0	n.d.	0.61	0.07	7	n.d.
Soil and extracts	Arid topsoil	P12	(-30) - 0	1.7	-0.14	0.06	6	n.d.
	Soil saturation extracts	P13	(-30) - 0	n.d.	0.54	0.10	6	n.d.
	Arid subsoil	P14	(-100) - (-30)	1.8	-0.24	0.07	6	n.d.
	Soil saturation extracts	P15	(-100) - (-30)	n.d.	0.48	0.08	6	n.d.

Note 1. K is translocated from soil pools to roots, between stem and leaves and then to dead leaves for tress and grasses, respectively. Note 2. The height below surface is marked using a negative value of the height above surface. Replicate run represents isotope analysis of sample aliquots through another column session. Note 3. "n.d.": not determined. 2 S.D. = two standard deviation; N = 1 the number of analytical cycles.  $\Delta^{41} K_{Plant-Source}$  value is calculated from  $\delta^{41} K_{Plant}$  subtracted by averaged  $\delta^{41} K_{Soil}$  saturation extracts, which is the mean value of  $\delta^{41} K_{Soil}$  saturation extracts of the topsoil and the subsoil.

sampling and we did not characterize organically bound K separately from the < 2-mm soil fraction.

The third suite of samples was used to assess K speciation and its isotopic composition within plant tissues. Samples include roots, stems, barks, aboveground shoots (a sum of stems and leaves), reproductive tissues (seeds and flowers), and leaves (fresh and dead leaves attached to grass stems or young branches) sampled during October 2018 and July 2019 (Table1). Individual specimens of grasses (P. setaceum and C. ciliaris) were sampled from the field and separated into reproductive tissues, leaves (live and dead), stems, and roots (without distinguishing between fine and coarse roots). The grass roots were partially collected. Tissues of trees (M. integrifolia and P. chilensis) were collected. Specifically, tree barks were sampled from small stems near the end of a branch at the height of  $\sim 1.5$  m, and tree leaves were sampled from branches within accessible height (~1.5 to 2 m). We note that tissues were not collected along the entire height of the tree. The root tissue and the cellulose-rich part of the heartwood were not collected as a part of this reconnaissance effort. Dead leaves were sampled from standing plants to avoid direct contact with soils to preclude K transfer from the K-rich soil to K-poor litter materials.

Collected tissues were rinsed using deionized water (Millipore<sup>TM</sup>,

 $18.2~\text{M}\Omega\cdot\text{cm}$ ) and then freeze-dried using liquid  $N_2$  treatments at the Phytotron, North Carolina State University. Tissues of the same plant type were homogeneously mixed to obtain the representative sample. Samples were powdered in a mortar with a pestle and weighted before analysis.

#### 3. Methodology

## 3.1. Extraction, digestion, and element analysis

Soil K residing in different chemically defined pools was determined through sequential treatment with progressively harsher chemical extractants. Four individual K fractions were extracted, including watersoluble K, K adsorbed onto clay surfaces, K interlayered within mica/illite (and/or halloysite), and K occluded within non-swelling silicate minerals (Cox et al.,1999). Soil water-soluble and exchangeable K were extracted using deionized water and 0.1 M NH<sub>4</sub>Ac, respectively. Interlayered K hosted into illite/mica and halloysite was quantified by sodium tetra-phenyl borate (NaBPh<sub>4</sub>) solutions (a mixture of 0.25 mol·L¹ NaBPh<sub>4</sub> + 1.7 mol·L¹ NaCl + 0.01 mol·L¹¹ EDTA, Cox et al.,1999). Soil occluded K was calculated by subtracting above three K fractions from

W. Li et al. Geoderma 400 (2021) 115219

soil total K pool. In addition, soil saturation extraction has been applied, and we used the  $\delta^{41}$ K of soil saturation extracts to approximate the  $\delta^{41}$ K of bioavailable pools. The extracts were obtained by mixing dry soil samples with deionized water until forming saturated pastes in equilibration and then treated with vacuum-filtration extraction (Soil Survey Laboratory Staff, 1992). Saturated paste extraction of soil is a standard chemistry procedure that produces more comparable results than watersoluble K extraction procedures, and is in the same state of equilibrium with respect to soil phases as soil solutions residing in soil during unsaturated stages (as opposed to macropore flow) (Burt, 1995). Hence, it likely reflects the chemistry properties of porewater for biological usage. Bioavailable K was derived from relatively concentrated basaltic substrate initially, but with continued weathering and rapid K leaching may reflect increasing contributions of mineral aerosols derived from dust accretion and relatively dilute marine aerosols over time (Chadwick et al. 1999).

To extract K adsorbed on outer root surfaces (including root extracellular excretion), roots were soaked in ice-cold 1 M HCl (5 °C, 40 g · L 1) for 3 min (Chaignon et al., 2002; Aucour et al., 2015). Besides extraction, fresh root tissues were digested using a mixture of 6 mL concentrated HNO<sub>3</sub> (sub-boiled distilled) and 2 mL 30% H<sub>2</sub>O<sub>2</sub> in Teflon beakers > 150 °C. Digested residues were evaporated and subsequently re-dissolved in 5 mL 2% HNO3 solution for chemical analyses (Tang et al., 2016). Soils were digested following a HCl-HNO<sub>3</sub>-HF protocol in Li et al. (2019b). Residues were converted to a nitric form by adding 2% HNO<sub>3</sub> solutions and measured using a quadrupole ICP-MS (Q-ICP-MS, Agilent<sup>TM</sup> 7900) at the University of North Carolina at Chapel Hill. Element analysis was calibrated by multi-elemental standards of known concentrations. Internal standards, including Be, Ge, Rh, In, Ir, and Bi, were used for instrument drift correction. Geostandards BHVO-2, GSP-2, SBC-1, and ERMBC382 were used to evaluate the accuracy and reproducibility (Table S1). External analytical accuracy<10% (2 S.D.) was achieved, and total yields (measured date relative to reported data) were satisfactory (100  $\pm$  5%).

#### 3.2. K Column chemistry

An aliquot of digested sample was evaporated to dryness and refluxed using 2 mL 0.7 M  $\rm HNO_3$  before loading onto the columns. Potassium isotopic compositions were measured after column purification, following the two-step purification approach reported in Chen et al. (2019). A first column was filled with 17 mL AG50-X8 cation-exchange resin (200-400 mesh, Bio-Rad<sup>TM</sup>) and conditioned in 0.7 M HNO<sub>3</sub>. Eluted K fractions were then collected after most of the matrix elements being eluted. Then collected K elution was evaporated until dryness on the hotplate and re-dissolved in 1 mL 0.5 M HNO<sub>3</sub> solution for the second column. The second column was filled with 2.4 mL AG50-X8 cationexchange resin (200–400 mesh, Bio-Rad  $^{\text{TM}}$ ) and conditioned in 0.5 M HNO<sub>3</sub>. After chromatographic processes, the fractions recovered before and after the collected volumes were checked for K, Na, Al, Fe, Rb, and Ti on the Agilent  $^{TM}$  7900 Q-ICP-MS. Collected fractions of K reached  $\sim$ 100% yields to exclude possible isotopic fractionation in ion-exchange chromatography. The mass ratios of a sum of all other matrix elements to K were measured to ensure a sum of matrix elements is below 2% of total K to reduce potential matrix effects on isotope analysis (Chen et al., 2019). If necessary, chromatographic processes were repeated to achieve acceptable matrix/K ratios for instrumental analysis. Column blanks were at least three orders of magnitude lower than the K mass used in the analytes. Procedural blanks (<5 ng) are negligible relative to total K mass (10-14 µg) used for instrumental analysis.

# 3.3. K Isotope analysis

For K isotope analysis using MC-ICP-MS, samples and bracketing standards were diluted using 3% HNO $_3$  to a K concentration of 5 to 8 mg·L $^{-1}$ , corresponding to  $^{39}$ K signals of 5 V to 11 V. The isotopic

compositions were measured using the Nu Plasma II HR- MC-ICP-MS at the Isotope Laboratory, University of Washington, Seattle. After digestion, samples were converted into a nitric form using 3% HNO3 and diluted to match a K concentration of 2 mg·L<sup>-1</sup>. Mass spectrometry and data processing were performed using established protocols (Hu et al., 2018; Xu et al., 2019). In brief, K isotopic ratios were measured with a high-resolution mode of "cool plasma" (low RF power from 750 to 850 W) to suppress interferences from residual and isobaric (<sup>40</sup>Ar<sup>1</sup>H<sup>+</sup> on <sup>41</sup>K<sup>+</sup> and <sup>38</sup>Ar<sup>1</sup>H<sup>+</sup> on <sup>39</sup>K<sup>+</sup>) argides. We used a dry plasma introduction system involving a CETAC Aridus II desolvation nebulizer system, a Savillex™ PFA spray chamber, and a C-Flow PFA microconcentric nebulizer, to reduce argide formation and increase sensitivity. On-peak zero for K mass 41 ranges between  $-8 \times 10^{-4}$  and  $-1.5 \times 10^{-3}$  V, approximating  $-3 \times 10^{-3}$  V for mass 39. These signals are negligible compared to the signal produced by samples (5 to 11 V). A standard bracketing method with over 5 cycles was adopted to correct instrumental mass bias. The K isotopic compositions were reported relative to NIST SRM 3141a with a  $\delta$  notation ( $\delta^{41}$ K, %) (Teng et al., 2017). The precision better than 0.12‰ was achieved based on repeated analyses of geostandards over a six-month period (2 S.D., Hu et al., 2018).

$$\delta^{41}K \ (\%ee) = \left\{ \frac{({}^{41}K/{}^{39}K)_{sample}}{({}^{41}K/{}^{39}K)_{NIST \ SRM \ 3141a}} - 1 \right\} \times 1000 \tag{1}$$

The "S.D." denotes the standard deviation over the analytical cycle of the sample. Several samples were measured twice via two separate analytical cycles, and averaged data are listed in Table 1. Two certified USGS standards (BHVO-2 and GSP-2) were processed in the same strategy and measured alongside samples for quality control and reproducibility evaluation. Potential systematic deviations among different laboratories for K isotope measurements could be alleviated by analyzing same reference materials (BHVO-2 and GSP-2). This study reports identical K isotope ratios of terrestrial igneous rocks within the analytical uncertainties, BHVO-2 of  $-0.40\pm0.06\%$  (2 S.D.) (a literature compilation from -0.52 to -0.40% ) and GSP-2 of  $-0.46\pm0.09\%$  (2 S. D.) (a literature compilation from -0.50 to -0.45%) (Table S2). Errors in the text reported as 2 S.D. are similar to or smaller than the reproducibility of in-house standards (Table 1). Without direct analysis, the isotopic compositions of the bulk plant and shoot can be calculated based on mass balance:

$$\delta^{41}K_{Bulk \ or \ shoot}(\%) = \frac{\sum_{i} mC_{i} \delta^{41}K_{i}}{\sum^{m} C_{i}}$$
 (2)

Where m represents the weight of dry mass (mg), c: K concentration (mg·L<sup>-1</sup>), and i: tissues of the bulk plant (root + stem + leaf + reproductive tissues) or shoot (stem + leaf).

## 3.4. K X-ray absorption analysis

The X-ray absorption fine structure (XAFS) spectra of K were collected for K references, powdered Hawaiian soils, and powdered plant tissues (frozen dried) at Soft X-ray Micro-Characterization Beamline (SXRMB, 06B1-1), Canadian Light Source (CLS, Saskatoon, Canada) under room temperature in the vacuum chamber to reduce beam attenuation. The beamline was equipped with Si drift fluorescence detectors and was monochromated with diffraction from InSb (111) and Si (111) double-crystals. In the photon energy range of K K-edge analysis (3550 to 4000 eV), the photon flux is about  $2 \times 10^{10}$  photon s<sup>-1</sup> (Li et al., 2020b), and the beam size at the target is  $\sim 7 \text{ mm} \times 1 \text{ mm}$  (Hu et al., 2010). The K-edge XAFS spectra of ionic K<sup>+</sup> in water (KCl solutions) were collected at the beamline 4-3 of the Stanford Synchrotron Radiation Lightsource (SSRL) using a fluorescence mode. This beamline was equipped with a 7-element fluorescence drift detector, an ionization chamber, and PIPS/Lytle detectors. Within the photon energy range of K *K*-edge analysis (3550 to 4000 eV), the photon flux is  $\sim 2 \times 10^{10}$  photon s<sup>-1</sup> at 100 mA, and the spot size is  $\sim$  7 mm  $\times$  1 mm. Powdered samples

were evenly spread as a thin film on double-sided K-free C tape adhered to a Cu stick before being placed in a vacuum chamber. Radiation damage was negligible, given satisfactory reproducibility. Two to four XAFS spectra were averaged to enhance signal-to-noise ratios in Athena software (Ravel and Newville, 2005).

The XAFS spectral changes are sensitive to the coordination environment of the element of interest, so they could help with phase identification. Spectral differences in K K-edge XAFS spectra of two references (i.e., K-pectate and ionic K+) and plant samples could be recognized (Fig. 1). The reason for this reference selection is that 1) pectate salts are the most well-known compounds responsible for K isotopic fractionation within plants, and 2) K is almost exclusively present in its ionic form within plant tissues (Bagard et al., 2013; Barker and Pilbeam, 2016). Fresh leaves exhibit a pronounced major peak at  $\sim$ 3616 eV, with slightly positive offsets in the major peak by  $\sim 1$  eV, in comparison with other tissues (Fig. 1a). Such a peak shift is observed in K XAFS spectra, corresponding to the spectral features of K-pectate and ionic K<sup>+</sup> (Fig. 1b). Nevertheless, the variations in photo energy and the k-space spectra are potentially affected by energy calibration. Another important change is the post-edge intensity, which can be identified by colored regions in Fig. 1 and is driven by electron gain or loss in the density of empty state in K (electron movement).

The atomic environments of K in fresh leaves and roots are very different from K phases preserved in stems, barks, and dead leaves. The differences could be explained by the mixing of two components – K-pectate and ionic  $K^+$ . According to the Natoli's rule – the energy dependence on average ligand shell radius (Natoli, 1984), variations in spectra highlights the decrease in the K-O distance in fresh leaves in comparison with remaining tissues. An absence of variations in the shape of K K-edge XANES spectra demonstrates that the coordination numbers of K atoms do not vary between K references. Compared to ionic  $K^+$ , fewer empty orbital states of K atoms in K-pectate (RCOO') exist with a lower electron donation capacity due to the electron reception of the O 2p-orbital, presumably reflecting a lower coordination number of K atoms in K-pectate. Moreover, a displacement of major energy peaks in the K XANES spectra between tissues can be identified

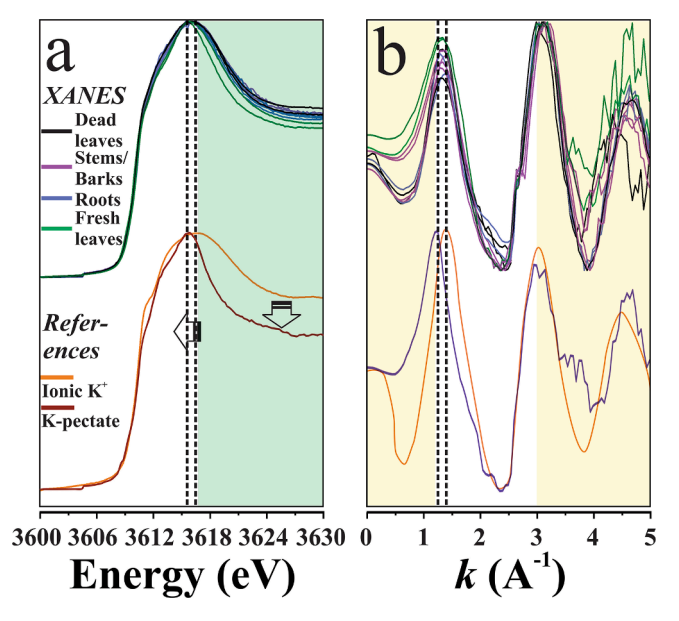


**Fig. 1.** K K-edge XAFS data including (a) XANES and (b) XAFS spectra in a k space of K references and plant tissues (leaves, stems, barks, and roots). References include K-pectate and ionic  $K^+$  (in water). The K XANES spectra of ionic  $K^+$  were collected in this study, and the XAFS spectra of ionic  $K^+$  obtained at 300 Kelvin refers to Glezakou et al. (2006). The dashed lines show slight peak shifts, the green area shows the discrepancy in the post-edge, and the yellow regions highlight changes linked to atomic coordination.

(Fig. 1).

There are two common methods for quantitative identification, i.e., spectral fitting of X-ray Absorption Near-Edge Structure (XANES, a part of XAFS near the absorption edge) and full K K-edge XAFS spectra. In this study, fitting was performed using K-pectate and ionic  $K^+$  spectra (Fig. 2). Only K K-edge XANES spectra were used for linear combination fitting since the full XAFS spectrum of ionic K was not obtained at the beamline. We used an R-factor to evaluate the goodness-of-fit. The significance between fits was determined using the Hamilton test (p < 0.05; Calvin, 2013) with a few independent data points calculated after normalization to a sum of 100%, estimated as data range divided by the core—hole lifetime broadening. Fits were accepted when a sum of percentages reached  $100\pm10\%$ .

#### 4. Results

#### 4.1. K In plant tissues

For grass tissues, the K concentration followed a sequence of fresh leaves > stems  $\approx$  reproductive tissues (flowers and seeds) > roots > dead leaves (Table 1). Aboveground shoots (a sum of stems and leaves) accumulated larger amounts of K than roots by  $\sim 10~g\cdot kg^{-1}$  in the humid site and  $\sim 5~g\cdot kg^{-1}$  in the arid site. Grasses (*P. Setaceum*) in the humid site showed higher tissue K concentrations compared with grasses (*C. Ciliaris*) in the arid site, by up to 15.3  $g\cdot kg^{-1}$  in fresh leaves (Fig. 3).

Using averaged  $\delta^{41} K$  of soil saturation extracts to approximate the  $\delta^{41} K$  of soil bioavailable pools, all grass tissues showed negative isotopic shifts from soil bioavailable pools, with  $\Delta^{41} K_{Plant-Source}$  of -0.89 to -0.25% (humid) and -0.86 to -0.04% (arid) Fig. 4). Isotopically light K was enriched in roots, showing  $\Delta^{41} K_{Root-Source}$  from -0.40 to -0.36% (P. Setaceum, humid) and -0.29 to -0.26% (C. Ciliaris, arid). Tissue  $\delta^{41} K$  data followed an order of fresh leaves > roots > stems > reproductive tissues > dead leaves (Fig. 5). Aboveground shoots (a sum of stems and leaves) were isotopically comparable to fresh leaves. The treatment of roots using HCl, which is assumed to extract K on the exterior of the roots, made up of 34% (humid) and 62% (arid) K in roots. The extraction provided  $\delta^{41} K$  values of 0.29  $\pm$  0.07% (humid) and 0.61  $\pm$  0.07% (arid), higher than soil bioavailable pools.

For tree tissues, the K concentration followed a sequence of fresh leaves > barks > dead leaves (Table 1). Fresh leaves of *M. integrifolia* in the humid site had lower concentrations of K compared with *P. chilensis* in the arid site by  $4.9 \, \mathrm{g \cdot kg^{-1}}$ .

Fresh leaves were isotopically heavier than barks and dead leaves in both sites. Similar to grass tissues, the lowest  $\delta^{41} K_{Plant}$  value was found in dead leaves (Figs. 4-5), and the enrichment of lighter K isotopes in dead leaves occurred in parallel with the reduction in K concentration. All tree tissues in the arid site exhibited negative  $\Delta^{41} K_{Plant\text{-}Source}$  values (-1.14 to -0.30%), while tree tissues in the humid site showed both negative and positive K isotopic shifts from soil bioavailable pools (-0.92 to 1.26%). In addition, the K isotopes in arid trees exhibited a smaller shift in  $\Delta^{41} K_{Plant\text{-}Source}$  values than in humid trees.

The K-pectate and ionic  $K^+$  in plants were identified by K K-edge XAFS spectra, based on spectral features (peak shifts and amplitudes, Fig. 1). According to XANES-LCF (Fig. 2), we quantified the following groups with distinct compositions of K-pectate and ionic  $K^+$ : (i) roots, (ii) stems (and barks), (iii) fresh leaves, and (iv) dead leaves. Grassroots and fresh leaves showed the highest proportions of K-pectate of 60–64% and 68–72%, respectively. Dead leaves exhibited the least proportions of K-pectate ranging from 42 to 50%. In grass stems, 53–56% of K was associated with pectate, and 44–47% of K presented as free ions. In tree barks, 53–55% of K was linked with pectate, and 45–47% of K existed as free ions.

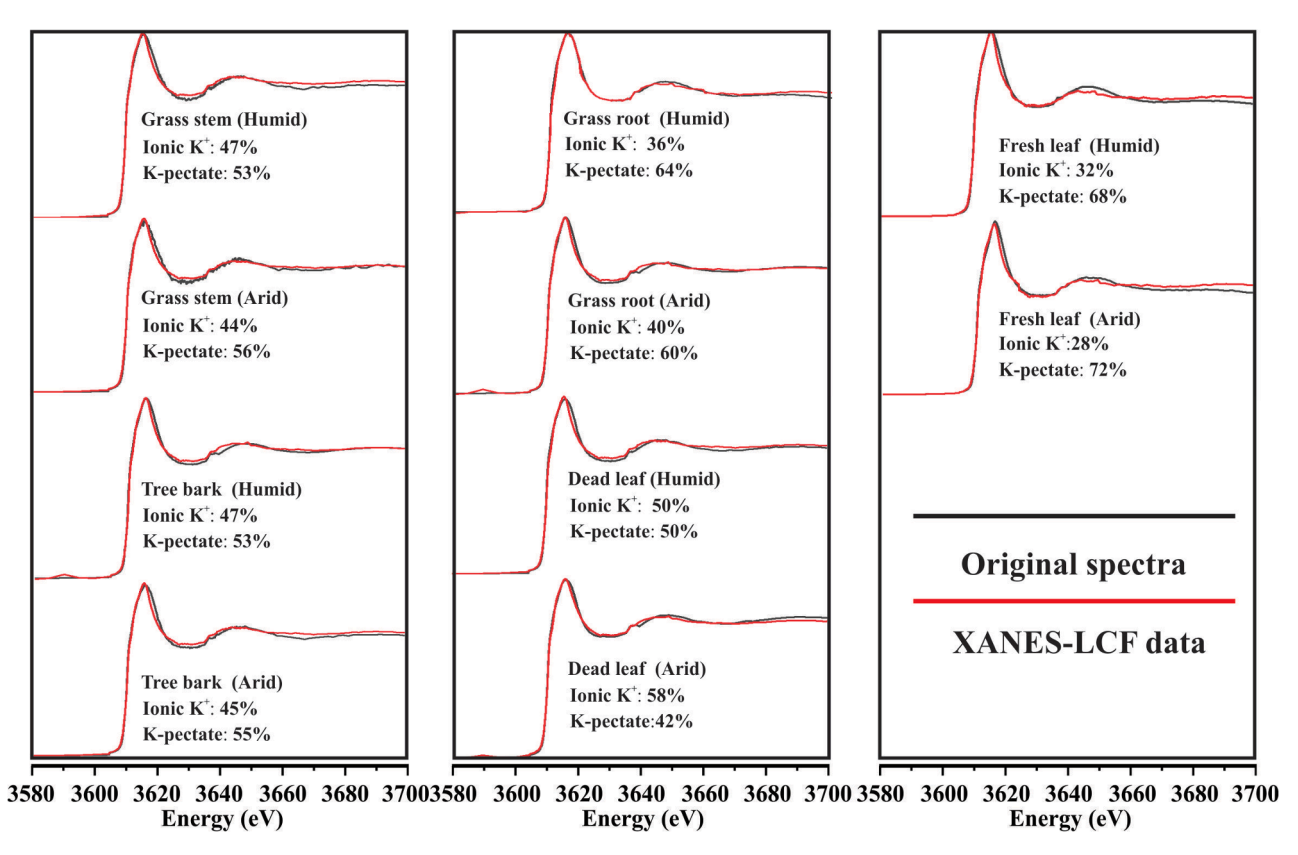


Fig. 2. Potassium K-edge XANES spectra of plant tissues from the humid (BE) and arid (PO) sites. The XANES spectra were subjected to linear combination fitting (XANES-LCF) based on reference compounds (i.e., ionic  $K^+$  and K-pectate, data from Fig. 1). The original spectra and LCF curves are marked in black and red, respectively.

#### 4.2. K In soils and waters

The K concentrations in soils and waters in the humid site were different from the arid site (Table 1 and Fig. 3). At the humid site, the K concentration (28.7  $g \cdot kg^{-1}$ ) in the topsoil (0–30 cm) was higher than those of the subsoil (30–100 cm) (8.7  $g \cdot kg^{-1}$ ) and the basaltic substrate (8.1  $g \cdot kg^{-1}$ ) (Table 1). The arid soil showed a reverse pattern in depth (1.7  $g \cdot kg^{-1}$  K in the topsoil and 1.8  $g \cdot kg^{-1}$  K in the subsoil).

The topsoil and subsoil in the humid site had comparable  $\delta^{41}$ K values of  $-0.49\pm0.06\%$  and  $-0.54\pm0.07\%$ , respectively. Soil  $\delta^{41}$ K values in the humid site were comparable to those of the basaltic substrate (e.g., Pololū lava,  $-0.48\pm0.04\%$ ; Hāwī tephra,  $-0.48\pm0.10\%$ ) and atmospherically derived mineral aerosols (e.g., Chinese loess JX-1,  $-0.46\pm0.05\%$ ) reported in Huang et al. (2020). The  $\delta^{41}$ K values of the arid soil (-0.14  $\pm$  0.06%, topsoil;  $-0.24\pm0.07\%$ , subsoil) were higher than those of the basaltic substrate and Asian-sourced mineral aerosols

For chemically-defined fractions in the topsoil, most soil-hosted K ( $\sim$ 36–59%) was fixed in occluded phases, and interlayered K made up  $\sim$  29–43% soil K. Soil exchangeable K (clay adsorbed) and water-soluble K were relatively less important, accounting for  $\sim$  7–10% and  $\sim$  4–13% soil K, respectively (Fig. 3). A marked difference in  $\delta^{41}$ K existed between the soil saturation extracts at the humid site (0.34  $\pm$  0.08‰, the topsoil;  $-0.63 \pm 0.08$ ‰, the subsoil). In comparison, the  $\delta^{41}$ K values of the soil saturation extracts at the arid site were identical (0.54  $\pm$  0.10‰, topsoil; 0.48  $\pm$  0.08‰, subsoil) within the analytical uncertainties. Based on field observation, the roots of trees and grasses were able to reach the bioavailable pool of the topsoil and subsoil. To derive a rough estimate of the K isotopic composition of soil bioavailable pool (source), we averaged the  $\delta^{41}$ K values of soil extracts of the topsoil and subsoil (Bullen and Chadwick, 2016). According to this assumption,  $\delta^{41}$ K values in soil bioavailable pools (averaged) were  $-0.15 \pm 0.08$ ‰ and 0.51  $\pm$ 

0.09‰ in humid and arid sites, respectively. Rainwater samples had  $\delta^{41}K$  values from  $-0.21\pm0.11$  to  $-0.16\pm0.07‰.$ 

#### 5. Discussion

## 5.1. Intra-plant K isotopic fractionation

During intra-plant circulation, the maximum isotopic fractionations between roots, leaves, and stems (barks) exhibit  $\Delta^{41}$ K values ranging from 0.82 to 2.17‰ for trees and 0.60 to 0.82‰ for grasses, respectively (Fig. 4). Therefore, intra-plant K isotopic fractionation is probably associated with ion-exchange processes along the transport pathway. Given the presence of K-pectate (Figs. 1-2), we infer that intra-plant K isotopic fractionation is linked to cation-exchange processes with the RCOO groups in the cell walls of xylem tissues. It is known that isotopic fractionation in chromatographic processes results in preferential complexation of isotopically heavier K with cation-exchange resin (rich in RCOO groups), producing large K isotopic fractionation up to 0.3% (Kawada et al., 1991; Xu et al., 2019). Accordingly, we anticipate that ion-exchange process during intra-plant circulation could induce heavier K isotopic compositions in roots and fresh leaves (rich in K-pectate) than stems (and barks) (rich in K<sup>+</sup>) (Fig. 6). This pattern is consistent with the observation that stems (and barks) are depleted in heavier K isotopes compared to the soil extraction and thus have heavier K isotopic composition in fresh leaves and roots (Fig. 5). This trend is obvious for sampled grasses while less evident for trees, probably due to a limited number (N = 2) of K K-edge XANES analysis of tree tissues, so further study is needed.

Lacking sufficient K-edge XAFS data of K references, we cannot exclude the co-existence of other organic-K phases in addition to K-pectate within plants. For example, in *Medicago truncatula* Gaertn. some K may remain lodged in fresh leaves as crystalline Ca-oxalate compound

W. Li et al. Geoderma 400 (2021) 115219

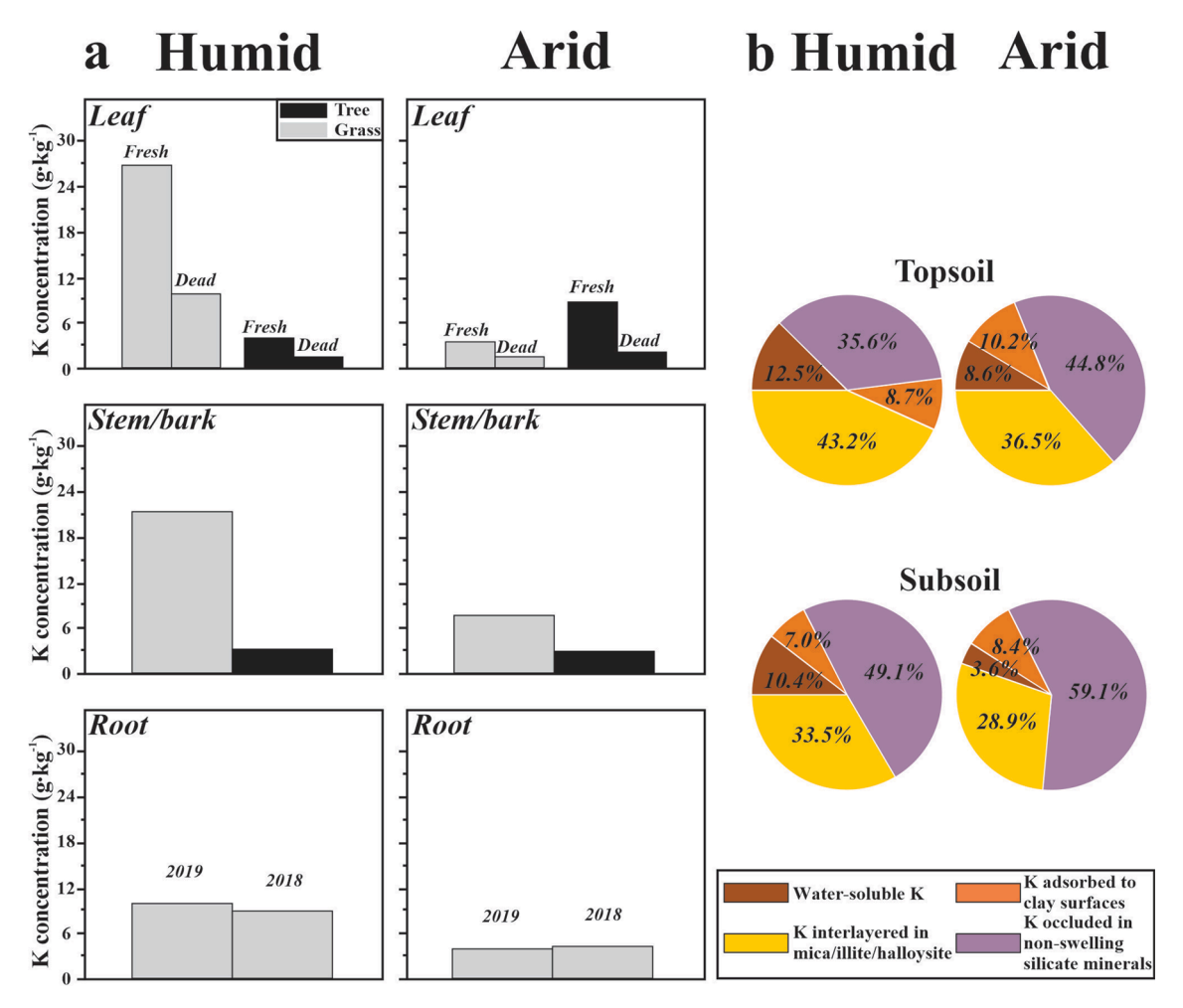


**Fig. 3.** Potassium concentrations in plant tissues and chemically defined soil fractions in the arid and humid sites in Hawai'i. (a) The K concentrations in the tissues of trees and grasses (*M. integrifolia* and *P. setaceum*) at the humid site, and the tissues of trees and grasses (*P. chilensis* and *C. ciliaris*) at the arid site. (b) The fractional distribution of K in the topsoil (0–30 cm) and subsoil (30–100 cm) at the humid and arid sites, respectively.

(whewellite,  $CaC_2O_4$ · $H_2O$ ) (Punshon et al., 2013). Even though not all plant K participates in intra-plant circulation, it appears that a portion of K forms mobile organic-K complexes such as K-pectate and this process leads to isotopically heavier K in roots and fresh leaves.

Substantial variations in tissue K concentration and its isotopic composition between litter and living biomass provide insights into K translocation within plants and into dead tissues (Fig. 4). Dead leaves exhibit lighter K isotopic composition compared to fresh leaves (Fig. 5). This difference can be better explained by K redistribution from the older leaves (poor in K-pectate) to younger tissues rich in (K-pectate). This interpretation is supported by the XANES- $\Delta^{41}$ K comparison (Fig. 6) that  $\Delta^{41}$ Kplant-Source is positively correlated to the percent of K-pectate. We also found that intra-plant K isotopic fractionation is comparatively large for sampled trees relative to grasses (Fig. 5). A possible explanation for this trend is that trees operate over longer time scales and transport distances than grasses, thus magnifying K isotopic fractionation by ion-exchange process during intra-plant circulation.

# 5.2. Root-soil K isotopic fractionation

Negative  $\Delta^{41}K_{Root\text{-}Source}$  values demonstrate that plants preferentially take up isotopically lighter K from soil bioavailable pools in the humid and arid systems (Table 1 and Fig. 5). This interpretation is consistent with recent results obtained from hydroponic experiments of several crops (Christensen et al., 2018). We suggest two driving forces responsible for plant preference for isotopically lighter K, including

adsorption on roots (and extracellular excretions of roots) and subsequent ion transport into root cells (Christensen et al., 2018).

Root adsorption is the retention of heavier K isotopes outside of root cells, leaving lighter K to be used by root cells. It could be supported by HCl leaching experiment of grassroots (Fig. 4), revealing that adsorption-driven K isotopic fractionation at the root-soil interface. The δ<sup>41</sup>K values of grassroot-HCl extracts are higher than those of untreated grassroots and soil saturation extracts (averaged) (Table 1), suggesting that K isotopic fractionation occurred before K entering the root cells. Therefore, K in roots is separated into two pools, a lighter pool utilized by plants and a heavier pool remained at root surface and gelatinous material on the exterior of the roots. The  $\delta^{41}K$  values of root residues after subtracting the contribution of K in root-HCl extracts based on K isotope mass balances. This calculation provides comparable  $\Delta^{41}$ K<sub>Resid</sub> values of -0.77% and -0.92% for humid and arid soils, respectively. We consider that near-constant K isotopic fractionations driven by root uptake of K probably indicate the same fractionation mechanism in both sites.

To maintain sufficient K concentration in cellular cytoplasm, K should be taken up by roots along the concentration gradient from the lower K<sup>+</sup> concentration external solution in soils (White and Karley, 2010). During root uptake, K isotopes can be fractionated (Christensen et al., 2018). Plant K<sup>+</sup> assimilation broadly involves a low-affinity (passive) transport path with ion-specific channels plus the electrogenic pump and a high-affinity (active) transport path using ion-specific carriers and the symporter system (Ashley et al., 2006). In general, the

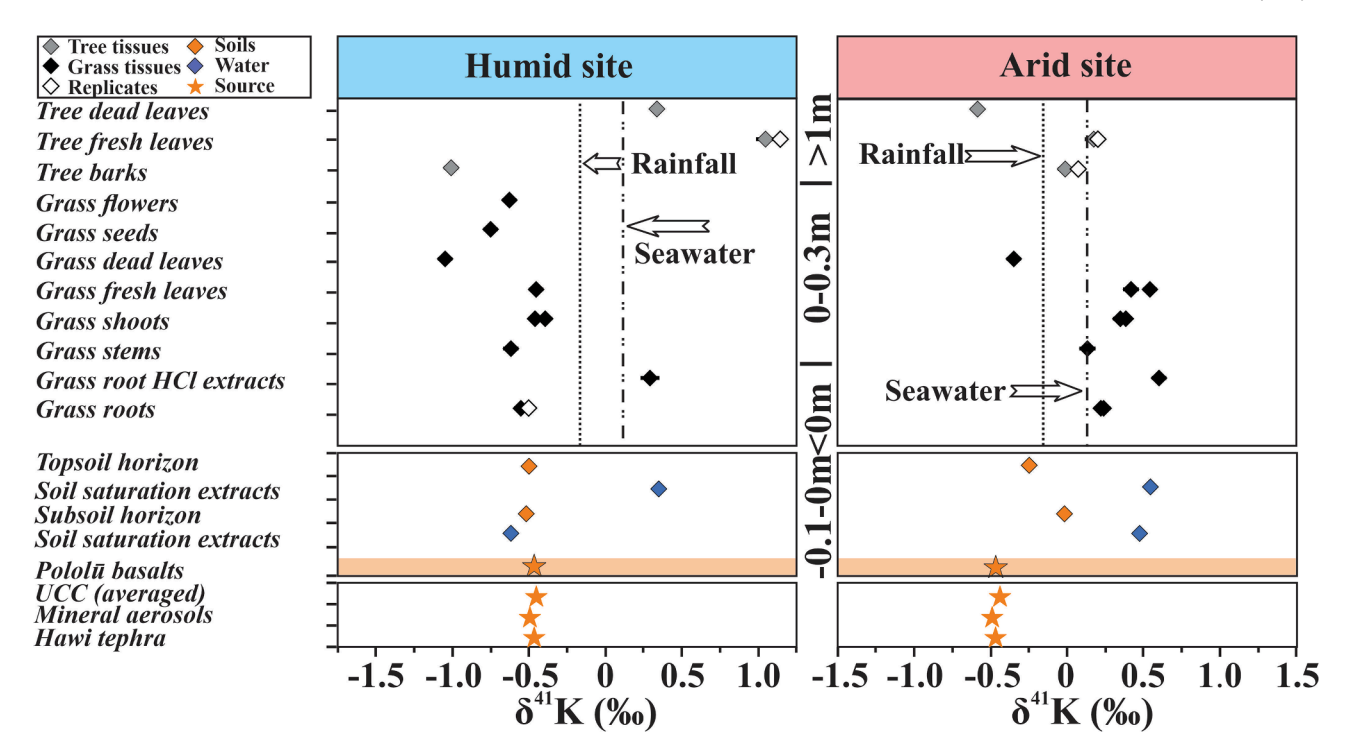


Fig. 4. The K isotopic compositions of tissue in trees and grasses (*M. integrifolia* and *P. setaceum*) in the humid site, and trees and grasses (*P. chilensis* and *C. ciliaris*) in the arid site, respectively (Table 1). Hollow diamonds represent duplicate analysis of tissue  $\delta^{41}$ K. Measured  $\delta^{41}$ K in bulk soils are symbolized by orange diamonds. The  $\delta^{41}$ K values of the basaltic substrate (Pololū basalt and Hāwī tephra), the upper continent crust (UCC, Huang et al., 2020), and dust-sourced mineral aerosols (Chinese loess JX-1, Huang et al., 2020) are plotted for comparison. The  $\delta^{41}$ K values of rainwater and seawater (Hille et al., 2019; Wang et al., 2020) are marked using dashed and dotted lines, respectively. The analytical uncertainties (2 S.D) of  $\delta^{41}$ K are smaller than the symbol sizes.

low-affinity transport path could be activated with high extracellular K concentrations (>1 mM) and the high-affinity transport path operates at low extracellular K concentrations (<1 mM) (e.g., Schachtman and Schroeder, 1994; Britto and Kronzucker, 2008). Because we did not collect porewater, soil saturation extracts may not fully represent temporal soil solutions. Another limitation is that K concentration in soil solutions may change over time; and therefore, the sampling period and amount of antecedent moisture may also matter.

Although the K concentration in soil solution cannot be robustly constrained, several lines of evidence demonstrate the low-affinity transport path is more important. Firstly, we use the K concentration in leaves of sampled plants compared with comparable plant species reported with sufficient K supplies to evaluate the abundance of soil bioavailable K. Here we assume that the physiological properties are similar to those of drought-enduring trees (Eucalyptus grandis W. Hill, and Eucalyptus urophylla S.T. Blake) of 8–20 g·kg<sup>-1</sup> (Rocha et al., 2019; Santos et al., 2020). Leaf K concentrations of trees (P. chilensis, 8.9 g·kg<sup>-1</sup>) in the arid site fall in a range with sufficient K supplies. Secondly, K is not considered as a limiting nutrient in Hawaiian soils based on fertilizer experiments using a dominant tree species (Metrosideros polymorpha Gaudich.) in Hawai'i (Vitousek and Farrington, 1997). Lastly, considerable  $\Delta^{41} K_{Residual \; root\text{-}Source}$  values for grass correspond to marked K isotopic fractionation driven by K transfer into roots. These values are comparable to an apparent K fractionation by about -1%produced by the size difference between <sup>39</sup>K and <sup>41</sup>K during K transport via ion channels (favored in the low-affinity path) (Christensen et al., 2018). As estimated in Christensen et al. (2018), the high-affinity transport path operated under low external K<sup>+</sup>, which would fractionate K isotopes much less than that of the low-affinity path. This highaffinity mechanism cannot reconcile measured  $\Delta^{41}K_{Residual\ Root-Source}$ close to -1%. In sum, we consider that the low-affinity, passive mechanism drives the K isotopic fractionation between soil bioavailable pools and plant roots in studied soil-plant systems.

## 5.3. K In soils and bioavailable pools

The isotopic variation of K in < 2-mm soils and saturation extracts fed by rainfall could be principally ascribed to source mixing of basaltic substrate, dust-derived mineral aerosols, and marine aerosols (Fig. 4). Collected rainwater has averaged  $\delta^{41}$ K value close to -0.18% (Table 1). Due to atmospheric processes, Asian-derived mineral aerosols may be partially dissolved in rain droplets, which was determined using radiogenic Sr isotopes of the same soil samples (Li et al., 2020a). The addition of mineral aerosols to the humid soil contribute substantial K to the soil pool because primary basaltic sources were depleted by leaching during weathering (Kurtz et al., 2001; Ryu et al., 2014). This argument is also supported by abundant quartz and mica (Li et al., 2020a) and interlayered K in these soils (K hosted in micaceous minerals derived from dusts, Fig. 3) (Merrill et al., 1994; Kurtz et al., 2001). Thus, despite intense weathering alteration, the humid soil shows  $\delta^{41}K$  values identical to those of mineral aerosols (Chinese loess,  $-0.46 \pm 0.05\%$ , Huang et al., 2020). Overall, the input of dust-derived mineral aerosols in soils likely masks the effect of basalt weathering that preferentially leaves light K isotopes in soils/regoliths (Chen et al., 2020; Teng et al., 2020).

Since K is a macronutrient, plant cycles (i.e., plant uptake and return of inorganic nutrients from depth to near soil surface) might add biological K in surface soils. Biologically utilized K is generally isotopically lighter than the source based on field observation in this study and hydroponic experiments (Christensen et al., 2018). Despite variations in plant covers and species in the humid and arid systems, we here provide two lines of evidence against marked plant imprints on soil K budget in both sites based on K isotopes.

First, we would expect a negative K isotopic shift in soils from the basaltic sources driven by plant cycling, which however, is not the case here (Fig. 3). An explanation is that the humid soil has  $\sim 90\%$  K hosted in silicates and plant imprints could be masked by mineral aerosols (Fig. 3). By contrast, the arid soil shows higher  $\delta^{41} K$  values compared with their potential sources – the Pololū lava and mineral aerosols,

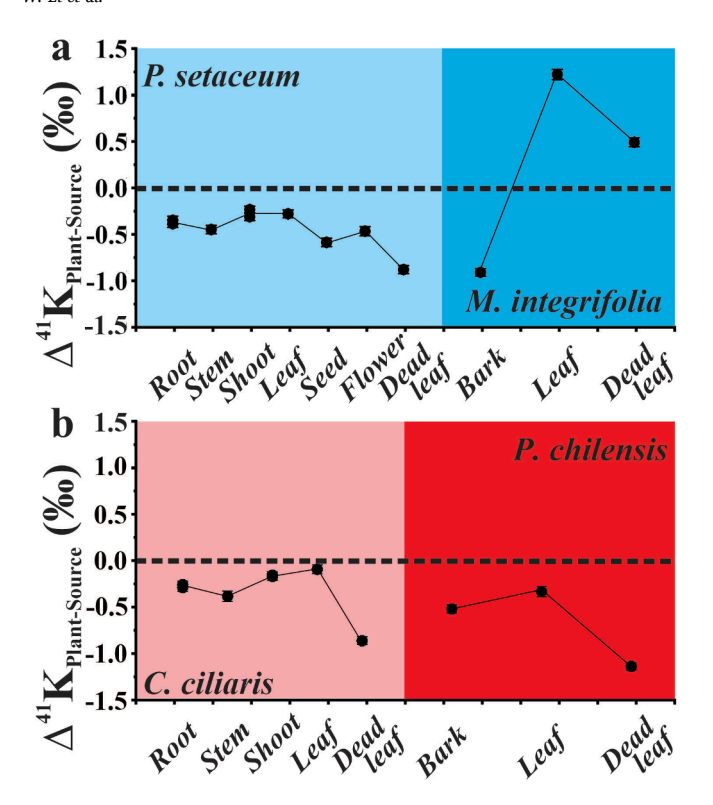
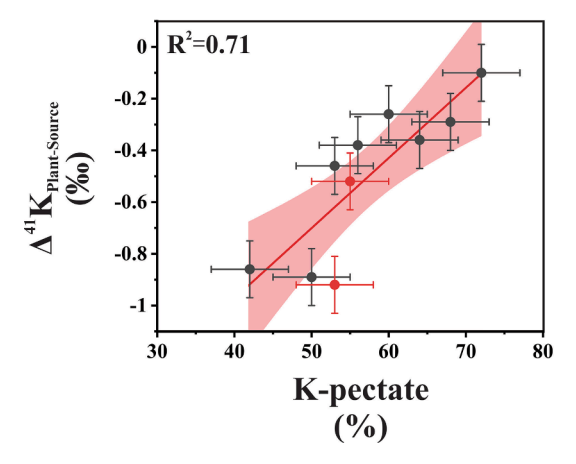


Fig. 5. The K isotopic compositions of plant tissues in comparison with averaged  $\delta^{41} K$  values of soil saturation extracts (taken as soil bioavailable pools and normalized to 0‰) from the (a) humid site and (b) arid site. Isotopically light K is preferentially taken up by grassroots from soil bioavailable pools. For intraplant K isotopic fractionation, the stem, seed, and flower of grasses are enriched in isotopically lighter K. Heavier K isotopes are preferentially accumulated in fresh leaves, while lighter K isotopes are enriched in dead leaves of trees and grasses in the study area.



**Fig. 6.** Potassium isotopic compositions in plant tissues versus the proportions of K-pectate based on XANES-LCF quantification (data depicted in Fig. 2). Tissue K isotopic compositions are normalized to the K compositions of soil saturation extracts (averaged) to assess intra-plant K isotopic fractionation. Measured grasses and trees are marked by grey and red, respectively. The error bars on the Y-axis represent the uncertainties of K isotope measurements (a long-term 2 S.D. value of 0.11‰, Hu et al., 2018), and the error bars on the X-axis represent the general uncertainty of the XANES-LCF approach (5%). A positive linear correlation can be observed ( $R^2 = 0.71$ ), and the red line denotes the linear fitting, and the red area covers the 95% confidence bands.

especially for the topsoil with a marked, positive isotopic offset of  $\sim$  0.4‰ from the basaltic substrate. High  $\delta^{41} K$  of the arid soil can be ascribed to the progressive accumulation of marine aerosols (using

 $\delta^{41}K_{Seawater}\sim0.14\%,$  Hille et al., 2019; Wang et al., 2020) due to higher evapotranspiration relative to precipitation (Goodfellow et al., 2014; Li et al., 2020a).

Moreover, saturation extracts are used to represent bioavailable pools. The  $\delta^{41}$ K values of saturation extracts differ between the topsoil and subsoil (Fig. 4). It is known that lighter K isotopes are preferentially taken by plants (Christensen et al., 2018 and this study) from bioavailable pools in the topsoil and subsoil, and then isotopically lighter K mostly returns to the topsoil pool once plants die and decay. Since plants take up K and then release again, constantly fractionating K, we expect K in the topsoil pool to be lighter than the subsoil pool over time. However, here we have not established full plant mass balance or the rate of K cycling. We did find however that  $\delta^{41}$ K values in the saturation extracts of the topsoil are more isotopically heavier than those of the subsoil in both sites (Fig. 4). Heavier K in topsoil saturation extracts likely have resulted from the dominance of marine aerosols, and K in subsoil saturation extracts might be regulated by weathering leaching. In summation, the concentration of K in soils should be much greater than the amount of K being added through plant cycling, and thus plantcycled fraction of total K is not large enough to affect the isotopic value

#### 6. Summary and conclusions

In Hawai'i, a wide variability in the K isotopic composition of plants reflects intra-plant and root-soil isotopic fractionations. Intra-plant K isotopic fractionation is regulated by cation-exchange processes. Plant tissues with higher proportions of organic-K association - K-pectate are more enriched in heavier K isotopes, causing higher  $\delta^{41}$ K values in roots and fresh leaves and lower  $\delta^{41}K$  in stems (and barks) and dead leaves. Intra-plant K isotopic fractionation is larger in trees compared with that of grasses, which could be ascribed to longer transport distances, and thus magnifying K isotopic fractionation during intra-plant circulation. At root-soil interfaces, adsorption onto root surface and extracellular excretion and lateral uptake in the root cells following a low-affinity transport pathway play important roles, which promote isotopically light K entering the root cells from soil bioavailable pools in both humid and arid sites. The variability of the K isotopic composition in bulk soils and saturation extracts mainly reflects mixing between the basaltic substrate and atmospheric deposition with limited influence from plants. The K isotopic composition of the humid soil is strongly influenced by atmospherically deposited mineral aerosols, which are rich in K-bearing minerals. In contrast, the isotopic compositions of marine aerosols could be well preserved in the arid soil due to relatively weak chemical leaching. The data demonstrate that stable K isotopes are a promising tool for understanding mechanisms of K utilization by plants and biogeochemical K cycling.

## **Declaration of Competing Interest**

The authors declare that they have no known competing financial interests or personal relationships that could have appeared to influence the work reported in this paper.

### Acknowledgements

The authors acknowledge funding support from the NSF Career Award (EAR-1848153) to X. M. Liu and Martin Research Fellowship from the University of North Carolina, Chapel Hill, to W.S. Li. We thank Jan Willem Van Groenigen for editorial handling and insightful feedbacks and two anonymous reviewers whose comments helped us improve the paper. We also thank Xikai Wang, Carole Saravitz and Mohsen Shakouri for technical assistance. The XAFS spectra were collected at the Canadian Light Source and Stanford Synchrotron Radiation Lightsource, with the approval of Proposal Review Committee (No. 30G09959, CLS) and (No. 10Z7, SSRL). Stanford Synchrotron Radiation

W. Li et al. Geoderma 400 (2021) 115219

Lightsource, SLAC National Accelerator Laboratory, is supported by U.S. Department of Energy, Office of Science, Office of Basic Energy Science. Canadian Light Source is supported by Canada Foundation for Innovation, Natural Sciences and Engineering Research Council of Canada, University of Saskatchewan, Government of Saskatchewan, Western Economic Diversification Canada, National Research Council Canada, and Canadian Institutes of Health Research.

#### Appendix A. Supplementary data

Supplementary data to this article can be found online at https://doi.org/10.1016/j.geoderma.2021.115219.

#### References

- Alexandre, A., Meunier, J.D., Colin, F., Koud, J.M., 1997. Plant impact on the biogeochemical cycle of silicon and related weathering processes. Geochim. Cosmochim. Acta 61, 677–682.
- Ashley, M.K., Grant, M., Grabov, A., 2006. Plant responses to potassium deficiencies: A role for potassium transport proteins. J. Exp. Bot. 57 (2), 425–436.
- Aucour, A.M., Bedell, J.P., Queyron, M., Magnin, V., Testemale, D., Sarret, G., 2015. Dynamics of Zn in an urban wetland soil-plant system: Coupling isotopic and EXAFS approaches. Geochim. Cosmochim. Acta 160, 55–69.
- An, Z., Liu, T., Lu, Y., Porter, S.C., Kukla, G., Wu, X., Hua, Y., 1990. The long-term paleomonsoon variation recorded by the loess-paleosol sequence in central China. Quat. Int. 7, 91–95.
- Bagard, M.L., Schmitt, A.D., Chabaux, F., Pokrovsky, O.S., Viers, J., Stille, P., Labolle, F., Prokushkin, A.S., 2013. Biogeochemistry of stable Ca and radiogenic Sr isotopes in a larch-covered permafrost-dominated watershed of Central Siberia. Geochim. Cosmochim. Acta 114, 169–187.
- Barker, A.V., Pilbeam, D.J., 2016. Handbook of plant nutrition. CRC Press.
- Burt R. (1995) Soil Survey Laboratory Information Manual. Soil Survey Investigations Report No. 45, USDA Soil Survey Laboratory.
- Becker, J.S., Füllner, K., Seeling, U.D., Fornalczyk, G., Kuhn, A.J., 2008. Measuring magnesium, calcium and potassium isotope ratios using ICP-QMS with an octopole collision cell in tracer studies of nutrient uptake and translocation in plants. Anal. Bioanal. Chem. 390, 571–578.
- Bolou-Bi, E.B., Poszwa, A., Leyval, C., Vigier, N., 2010. Experimental determination of magnesium isotope fractionation during higher plant growth. Geochim. Cosmochim. Acta 74, 2523–2537.
- Britto, D.T., Kronzucker, H.J., 2008. Cellular mechanisms of potassium transport in plants. Physiol. Plant. 133 (4), 637–650.
- Bullen, T., Chadwick, O., 2016. Ca, Sr and Ba stable isotopes reveal the fate of soil nutrients along a tropical climosequence in Hawaii. Chem. Geol. 422, 25–45.
- Caldelas, C., Dong, S., Araus, J.L., Jakob, Weiss D., 2011. Zinc isotopic fractionation in Phragmites australis in response to toxic levels of zinc. J. Exp. Bot. 62, 2169–2178.
- Capo, R.C., Whipkey, C.E., Blachère, J.R., Chadwick, O.A., 2000. Pedogenic origin of dolomite in a basaltic weathering profile, Kohala peninsula. Hawaii. *Geology* 28, 271–274.
- Chadwick, O.A., Derry, L.A., Vitousek, P.M., Huebert, B.J., Hedin, L.O., 1999. Changing sources of nutrients during four million years of ecosystem development. Nature 397 (6719), 491–497.
- Chadwick, O.A., Gavenda, R.T., Kelly, E.F., Ziegler, K., Olson, C.G., Crawford, Elliott W., Hendricks, D.M., 2003. The impact of climate on the biogeochemical functioning of volcanic soils. Chem. Geol. 202, 195–223.
- Chaignon, V., Bedin, F., Hinsinger, P., 2002. Copper bioavailability and rhizosphere pH changes as affected by nitrogen supply for tomato and oilseed rape cropped on an acidic and a calcareous soil. Plant Soil 243, 219–228.
- Chaudhuri, S., Clauer, N., Semhi, K., 2007. Plant decay as a major control of river dissolved potassium: A first estimate. Chem. Geol. 243, 178–190.
- Chen, H., Tian, Z., Tuller-Ross, B., Korotev, R.L., Wang, K., 2019. High-precision potassium isotopic analysis by MC-ICP-MS: An inter-laboratory comparison and refined K atomic weight. J. Anal. At. Spectrom. 34, 160–171.
- Chen, H., Liu, X.M., Wang, K., 2020. Potassium isotope fractionation during chemical weathering of basalts. Earth Planet. Sci. Lett. 539, 116192.
- Christensen, J.N., Qin, L., Brown, S.T., Depaolo, D.J., 2018. Potassium and calcium isotopic fractionation by plants (soybean [Glycine max], rice [Oryza sativa], and wheat [Triticum aestivum]). ACS Earth Sp. Chem. 2, 745–752.
- Cobert, F., Schmitt, A.D., Bourgeade, P., Labolle, F., Badot, P.M., Chabaux, F., Stille, P., 2011. Experimental identification of Ca isotopic fractionations in higher plants. Geochim. Cosmochim. Acta 75, 5467–5482.
- Cox, A.E., Joern, B.C., Brouder, S.M., Gao, D., 1999. Plant-available potassium assessment with a modified sodium tetraphenylboron method. Soil Sci. Soc. Am. J. 63, 902–911.
- Moynier, F., Hu, Y., Wang, K., Zhao, Y., Gérard, Y., Deng, Z., Moureau, J., Li, W.Q., Simon, J.I., Teng, F.Z., 2021. Potassium isotopic composition of various samples using a dual-path collision cell-capable multiple-collector inductively coupled plasma mass spectrometer. Nu instruments Sapphire. *Chem. Geol.* 571, 120144.
- Giambelluca, T.W., Chen, Q., Frazier, A.G., Price, J.P., Chen, Y.L., Chu, P.S., Eischeid, J. K., Delparte, D.M., 2013. Online rainfall atlas of Hawai'i. Bull. Am. Meteorol. Soc. 94, 313–316.

Glezakou, V.A., Chen, Y., Fulton, J.L., Schenter, G.K., Dang, L.X., 2006. Electronic structure, statistical mechanical simulations, and EXAFS spectroscopy of aqueous potassium. Theor. Chem. Acc. 115, 86–99.

- Goodfellow, B.W., Chadwick, O.A., Hilley, G.E., 2014. Depth and character of rock weathering across a basaltic-hosted climosequence on Hawai'i. Earth Surf. Process. Landforms 39, 381–398.
- Guelke, M., Von Blanckenburg, F., 2007. Fractionation of stable iron isotopes in higher plants. Environ. Sci. Technol. 41, 1896–1901.
- Hille, M., Hu, Y., Huang, T.Y., Teng, F.Z., 2019. Homogeneous and heavy potassium isotopic composition of global oceans. Sci. Bull. 64, 1740–1742.
- Holmqvist, J., Øgaard, A.F., Öborn, I., Edwards, A.C., Mattsson, L., Sverdrup, H., 2003. Application of the profile model to estimate potassium release from mineral weathering in Northern European agricultural soils. Eur. J. Agron. 20 (1–2), 149–163.
- Hu, Y., Chen, X.Y., Xu, Y.K., Teng, F.Z., 2018. High-precision analysis of potassium isotopes by HR-MC-ICPMS. Chem. Geol. 493, 100–108.
- Hu, Y.F., Coulthard, I., Chevrier, D., Wright, G., İgarashi, R., Sitnikov, A., Yates, B.W., Hallin, E.L., Sham, T.K., Reininger, R., 2010. Preliminary commissioning and performance of the soft x-ray micro-characterization beamline at the Canadian light source. In: In AIP Conference Proceedings, pp. 343–346.
- Huang, T.Y., Teng, F.Z., Rudnick, R.L., Chen, X.Y., Hu, Y., Liu, Y.S., Wu, F.Y., 2020.
  Heterogeneous potassium isotopic composition of the upper continental crust.
  Geochim. Cosmochim. Acta 278, 122–136.
- Humayun, M., Koeberl, C., 2004. Potassium isotopic composition of Australasian tektites. Meteorit. Planet. Sci. 39, 1509–1516.
- Humayun, M., Clayton, R.N., 1995. Precise determination of the isotopic composition of potassium: Application to terrestrial rocks and lunar soils. Geochim. Cosmochim. Acta 59 (10), 2115–2130.
- Jouvin, D., Weiss, D.J., Mason, T.F.M., Bravin, M.N., Louvat, P., Zhao, F., Ferec, F., Hinsinger, P., Benedetti, M.F., 2012. Stable isotopes of Cu and Zn in higher plants: Evidence for Cu reduction at the root surface and two conceptual models for isotopic fractionation processes. Environ. Sci. Technol. 46, 2652–2660.
- Kawada, K., Ol, T., Hosoe, M., Kakihana, H., 1991. Fractionation of potassium isotopes in cation-exchange chromatography. J. Chromatogr. A 538, 355–364.
- Kopáček, J., Turek, J., Hejzlar, J., Šantrůčková, H., 2009. Canopy leaching of nutrients and metals in a mountain spruce forest. Atmos. Environ. 43, 5443–5453.
- Kurtz, A.C., Derry, L.A., Chadwick, O.A., 2001. Accretion of Asian dust to Hawaiian soils: Isotopic, elemental, and mineral mass balances. Geochim. Cosmochim. Acta 65, 1971–1983.
- Li, S., Li, W., Beard, B.L., Raymo, M.E., Wang, X., Chen, Y., Chen, J., 2019a. K isotopes as a tracer for continental weathering and geological K cycling. Proc. Natl. Acad. Sci. U. S. A. 116, 8740–8745.
- Li, W., 2017. Vital effects of K isotope fractionation in organisms: observations and a hypothesis. Acta Geochim. 36, 374–378.
- Li, W., Beard, B.L., Li, S., 2016. Precise measurement of stable potassium isotope ratios using a single focusing collision cell multi-collector ICP-MS. J. Anal. At. Spectrom. 31, 1023–1029.
- Li, W., Liu, X.M., Godfrey, L.V., 2019b. Optimisation of lithium chromatography for isotopic analysis in geological reference materials by MC-ICP-MS. Geostand. Geoanalytical Res. 43, 261–276.
- Li, W., Liu, X.M., Chadwick, O.A., 2020a. Lithium isotope behavior in Hawaiian regoliths: Soil-atmosphere-biosphere exchanges. Geochim. Cosmochim. Acta 285, 175–192.
- Li, W., Liu, X.M., Hu, Y., 2020b. Potassium and calcium K-edge XANES in chemical compounds and minerals: Implications for geological phase identification. Geostand. Geoanalytical Res. 44 (4), 805–819.
- Li, W., Liu, X.M., Wang, K., Koefoed, P., 2021a. Lithium and potassium isotope fractionation during silicate rock dissolution: An experimental approach. *Chem. Geol.* 568, 120142.
- Li, W., Liu, X.M., Hu, Y., Teng, F.Z., Hu, Y.F., 2021b. Potassium isotopic fractionation during clay adsorption. *Geochim. Cosmochim. Acta* (in press). https://doi.org/ 10.1016/j.gca.2021.04.027.
- Li, X., Han, G., Zhang, Q., Miao, Z., 2020c. Optimal separation method for high-precision K isotope analysis by using MC-ICP-MS with a dummy bucket. J. Anal. At. Spectrom. 35 (7), 1330–1339.
- Merrill, J., Arnold, E., Leinen, M., Weaver, C., 1994. Mineralogy of aerolian dust reaching the North Pacific Ocean 2. Relationship of mineral assemblages to atmospheric transport patterns. J. Geophys. Res. 99, 21025–21032.
- Morgan, L.E., Santiago Ramos, D.P., Davidheiser-Kroll, B., Faithfull, J., Lloyd, N.S., Ellam, R.M., Higgins, J.A., 2018. High-precision <sup>41</sup>K/<sup>39</sup>K measurements by MC-ICP-MS indicate terrestrial variability of δ<sup>41</sup>K. J. Anal. At. Spectrom. 33, 175–186.
- Murphy, K.E., Long, S.E., Rearick, M.S., Ertas, Ö.S., 2002. The accurate determination of potassium and calcium using isotope dilution inductively coupled "cold" plasma mass spectrometry. J. Anal. At. Spectrom. 17, 469–477.
- Punshon, T., Tappero, R., Ricachenevsky, F.K., Hirschi, K., Nakata, P.A., 2013.
  Contrasting calcium localization and speciation in leaves of the Medicago truncatula mutant cod5 analyzed via synchrotron X-ray techniques. Plant J. 76, 627–633.
- Rocha J. H. T., Gonçalves J. L. de M., Ferraz A. de V., Poiati D. A., Arthur Junior J. C. and Hubner A. (2019) Growth dynamics and productivity of an Eucalyptus grandis plantation under omission of N, P, K Ca and Mg over two crop rotation. For. Ecol. Manage. 447, 158–168.
- Ryu, J.S., Vigier, N., Lee, S.W., Lee, K.S., Chadwick, O.A., 2014. Variation of lithium isotope geochemistry during basalt weathering and secondary mineral transformations in Hawaii. Geochim. Cosmochim. Acta 145, 103–115.
- Santiago Ramos, D.P., Morgan, L.E., Lloyd, N.S., Higgins, J.A., 2018. Reverse weathering in marine sediments and the geochemical cycle of potassium in seawater: Insights

- from the K isotopic composition (  $^{41}{\rm K}/^{39}{\rm K})$  of deep-sea pore-fluids. Geochim. Cosmochim. Acta 236, 99–120.
- Santos, E.F., Mateus, N.S., Rosário, M.O., Garcez, T.B., Mazzafera, P., Lavres, J., 2020. Enhancing potassium content in leaves and stems improves drought tolerance of eucalyptus clones. Physiol. Plant. 1–12.
- Sardans, J., Peñuelas, J., 2015. Potassium: A neglected nutrient in global change. Glob. Ecol. Biogeogr. 24, 261–275.
- Soil Survey Staff, 2014. Keys to Soil Taxonomy, 12th ed. USDA-Natural Resources Conservation Service, Washington, DC.
- Schachtman, D.P., Schroeder, J.I., 1994. Structure and transport mechanism of a highaffinity potassium uptake transporter from higher plants. Nature 370, 655–658.
- Schmitt, A.D., Cobert, F., Bourgeade, P., Ertlen, D., Labolle, F., Gangloff, S., Badot, P.M., Chabaux, F., Stille, P., 2013. Calcium isotope fractionation during plant growth under a limited nutrient supply. Geochim. Cosmochim. Acta 110, 70–83.
- Song, Z., Wang, H., Strong, P.J., Li, Z., Jiang, P., 2012. Plant impact on the coupled terrestrial biogeochemical cycles of silicon and carbon: Implications for biogeochemical carbon sequestration. Earth-Science Rev. 115, 319–331.
- Spengler, S.R., Garcia, M.O., 1988. Geochemistry of the Hawi lavas, Kohala Volcano. Hawaii. Contrib. to Mineral. Petrol. 99, 90–104.
- Soil Survey Laboratory Staff. (1992) Soil survey laboratory methods manual. Soil Survey Investigations Report. No.42. USDA-SCS, National Soil Survey Center, Lincoln, NE.
- Tang, Y.T., Cloquet, C., Deng, T.H.B., Sterckeman, T., Echevarria, G., Yang, W.J., Morel, J.L., Qiu, R.L., 2016. Zinc isotope fractionation in the hyperaccumulator noccaea caerulescens and the nonaccumulating plant Thlaspi arvense at Low and High Zn Supply. Environ. Sci. Technol. 50, 8020–8027.
- Teng, F.Z., Dauphas, N., Watkins, J.M., 2017. Non-Traditional Stable Isotopes: Retrospective and Prospective. Non-Traditional Stable Isotopes Walter de Gruyter GmbH 1-26
- Teng, F.Z., Hu, Y., Ma, J.L., Wei, G.J., Rudnick, R.L., 2020. Potassium isotope fractionation during continental weathering and implications for global K isotopic balance. Geochim. Cosmochim. Acta 278, 261–271.

Tripler, C.E., Kaushal, S.S., Likens, G.E., Todd, Walter M., 2006. Patterns in potassium dynamics in forest ecosystems. Ecol. Lett. 9, 451–466.

Geoderma 400 (2021) 115219

- Uhlig, D., Amelung, W., von Blanckenburg, F., 2020. Mineral nutrients sourced in deep regolith sustain long-term nutrition of mountainous temperate forest ecosystems. Global Biogeochem. Cycles 34 (9).
- Vitousek, P.M., Chadwick, O.A., 2013. Pedogenic thresholds and soil process domains in basalt-derived soils. Ecosystems 16 (8), 1379–1395.
- Vitousek, P.M., Farrington, H., 1997. Nutrient limitation and soil development: experimental test of a biogeochemical theory. Biogeochemistry 37 (1), 63–75.
- Vogel, C., Helfenstein, J., Massey, M.S., Sekine, R., Kretzschmar, R., Beiping, L., Peter, T., Chadwick, O.A., Tamburini, F., Rivard, C., Herzel, H., Adam, C., Pradas del Real, A. E., Castillo-Michel, H., Zuin, L., Wang, D., Felix, R., Lasalle-Kaiser, B., Frossard, E., 2021. Microspectroscopy reveals dust-derived apatite grains in acidic, highly weathered Hawaiian soils. Geoderma 381, 114681.
- White, P., Karley, A., 2010. Cell biology of metals and nutrients. In: Plant Cell Monographs. Springer, Berlin, pp. 199–224.
- Wang, K., Close, H.G., Tuller-Ross, B., Chen, H., 2020. Global average potassium isotope composition of modern seawater. ACS Earth Space Chem. 4 (7), 1010–1017.
- Whipkey, C.E., Capo, R.C., Chadwick, O.A., Stewart, B.W., 2000. The importance of sea spray to the cation budget of a coastal Hawaiian soil: a strontium isotope approach. Chem. Geol. 168 (1–2), 37–48.
- Weis, J.S., Weis, P., 2004. Metal uptake, transport and release by wetland plants: Implications for phytoremediation and restoration. Environ. Int. 30, 685–700.
- Weiss, D.J., Mason, T.F.D., Zhao, F.J., Kirk, G.J.D., Coles, B.J., Horstwood, M.S.A., 2005. Isotopic discrimination of zinc in higher plants. New Phytol. 165, 703–710.
- Xu, Y.K., Hu, Y., Chen, X.Y., Huang, T.Y., Sletten, R.S., Zhu, D., Teng, F.Z., 2019. Potassium isotopic compositions of international geological reference materials. Chem. Geol. 513, 101–107.
- Ziegler, K., Chadwick, O.A., Brzezinski, M.A., Kelly, E.F., 2005. Natural variation of  $\delta^{30}$ Si ratios during progressive basalt weathering. Hawaiian Islands. *Geochim Cosmochim Acta* 69 (19), 4597–4610.